Polarization-Dependent Curvature Loss in Silicon Rib Waveguides

Michael Krause, *Student Member, IEEE*, Hagen Renner, and Ernst Brinkmeyer

***Abstract*—We show that the quasi-TM mode in silicon rib waveguides can experience significantly less curvature loss at the same bend radius than does the quasi-TE mode. Photonic devices making use only of the TM mode and a polarization-diversity scheme can, thus, profit from smaller possible bend radii and the resulting circuit-size reduction. The main loss mechanism for the quasi-TM rib mode can be coupling to the orthogonally polarized TE slab mode, which radiates power away from the waveguide. This is possible due to the slight hybridicity of the quasi-TM rib mode. Neglecting this hybridicity would lead to a significant underestimation of the curvature losses. Thus, accurate simulation of waveguides with low quasi-TM-mode curvature loss requires full-vectorial simulation models.**

***Index Terms*—Curvature loss, integrated optics, leaky modes, rib waveguides.**

I. Introduction

THE basic building block for any photonic integrated circuit is the optical waveguide. In silicon photonics, practical single-mode waveguides with low propagation losses can be realized in various forms. Strip waveguides or "photonic wires" have a silicon core with cross-sectional dimensions of the order of a few hundred nanometers and are surrounded everywhere by a low refractive index material, namely, the silica buffer layer below and air or silica above [1]–[3]. On the other hand, rib waveguides have a larger core of the order of micrometers, as well as adjacent slabs of silicon on both sides. In spite of their large core dimensions, rib waveguides can be designed such that they guide only the fundamental mode, while all the higher order modes are leaky and radiate power through the adjacent slab waveguides [4]–[6]. Finally, photonic-crystal waveguides have been demonstrated, where light is guided along a line defect in a photonic-crystal slab [2], [7], [8].

Of all these waveguide types, rib waveguides pose the weakest requirements on the processing technology due to their relatively large dimensions. Furthermore, coupling light between the rib waveguides and the optical fibers is relatively easy, and rib waveguides can be designed to have low or even zero birefringence. In fact, achieving birefringence-free silicon rib waveguides has been the subject of recent research [6], [9]. In order to obtain fully polarization-independent operation, however, polarization-dependent loss (PDL) must also be kept low.

In this paper, we show that the waveguide bends can be a major source of PDL. The (quasi-)TE and TM modes of a rib waveguide experience curvature losses that can differ by orders of magnitude. In the silicon-on-insulator rib waveguides analyzed here, the loss of the TE mode is significantly larger than that of the TM mode at the same bend radius. Therefore, the minimal allowed bend radius for low-PDL operation is limited by the onset of the TE-mode curvature loss. An alternative solution to the problem of polarization dependence would be the use of a polarization-diversity scheme, where the two polarizations at the input of the device are split and each polarization is processed by its own circuit. At the output of the device, both polarizations are recombined again [2]. If such a scheme made use of only the TM mode of the rib waveguides, much smaller bend radii could be used, and the resulting circuit-size reduction could more than make up for the chip-area loss due to the required duplication of the circuit.

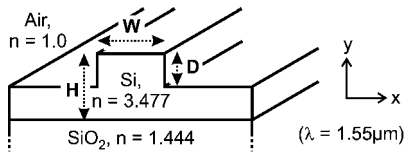

Fig. 1. Cross section of a silicon rib waveguide.

Finally, we show that full-vectorial waveguide models such as [10], [11] are essential for the design of silicon rib waveguides with low TM-mode curvature loss. Scalar [12], semivectorial [13], [14], or effective-index models [15] can significantly underestimate the curvature losses of the quasi-TM mode, because they do not allow for coupling of the quasi-TM rib mode to the radiating TE slab modes, which may be the principal curvature-loss mechanism.

II. Modeling

Fig. 1 shows the cross section of the rib waveguide analyzed in the following paragraphs as well as the material parameters used in the simulations. A central rib of height H and width W is surrounded by slab waveguides of height $H - D$, where D is the etch depth.

We have used a full-vectorial finite-difference mode solver in order to calculate the complex mode fields and propagation constants of guided and leaky modes of the rib waveguides [11]. We use a formulation in terms of the two transverse H-field components. The Helmholtz equation is solved in cylindrical coordinates, where the angular coordinate corresponds to the propagation direction in the curved waveguide. Perfectly matched layers (PMLs) are introduced through a complex coordinate transform [16] in order to allow for outgoing radiation. The method described in [17] was used to derive first-order

Manuscript received October 31, 2005; revised August 9, 2006.

The authors are with the Technische Universität Hamburg-Harburg, Optische Kommunikationstechnik, D-21073 Hamburg, Germany (e-mail: m.krause@tu-harburg.de; renner@tu-harburg.de; brinkmeyer@tu-harburg.de).

Digital Object Identifier 10.1109/JSTQE.2006.884068

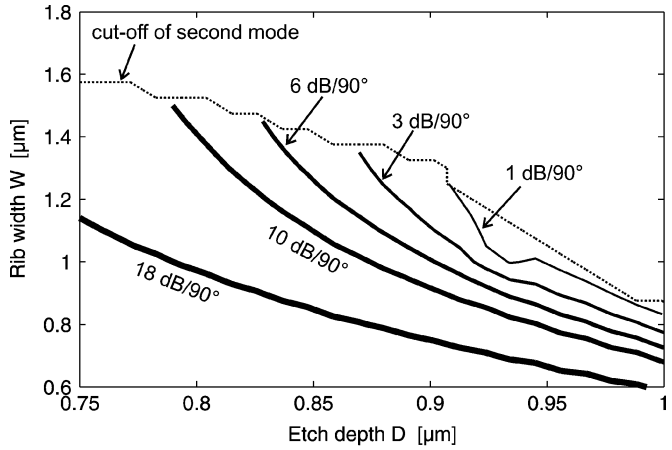

(a)

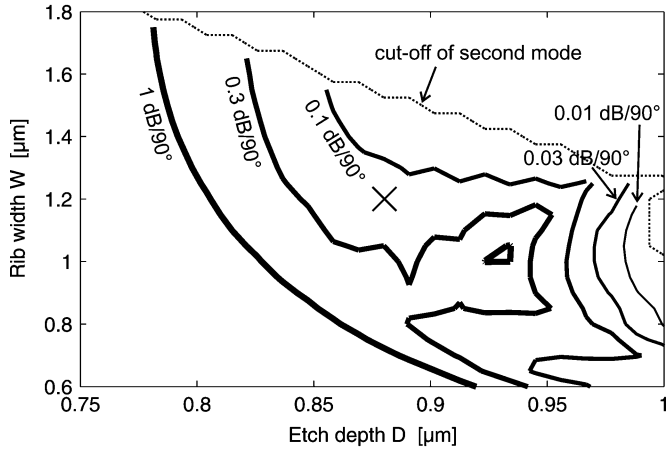

(b)

Fig. 2. Curvature loss for rib waveguides with height $H = 1.5$ μm in a 90° bend at the bend radius $R = 48$ μm. (a) TE mode. (b) TM mode.

(six point) finite-difference expressions for the differential operators. The formulas for four different choices of the six grid points are then averaged to obtain a symmetric formulation. The loss per 90° bend is calculated from the imaginary part of the complex propagation constant.

III. Curvature Loss in Silicon Rib Waveguides

A. Survey of the TE- and TM-Mode Losses

Fig. 2(a) shows the curvature loss of the fundamental quasi-TE mode of silicon rib waveguides for a 90° bend section with the bend radius $R = 48$ μm. The rib height has been kept fixed at $H = 1.5$ μm, and the rib width W and the etch depth D have been varied. None of the analyzed waveguides exhibit losses less than 1 dB per 90° bend. In contrast, the losses for the quasi-TM mode are much lower. They are shown in Fig. 2(b) at the same bend radius $R = 48$ μm. In a wide range of waveguide widths W and etch depths D, the curvature losses for the quasi-TM mode have acceptable values below 0.1 dB/90°.

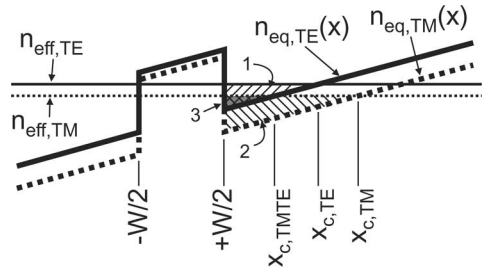

Fig. 3. Schematic effective-index model illustrating the three curvature-loss mechanisms. The three triangular areas visualize the tunneling barriers for radiation (1: *hatched* along SW–NE, from the TE rib mode to the TE slab mode; 2: *hatched* along NW–SE, from the TM rib mode to the TM slab mode; 3: their intersection marked in *gray color*, from the TM rib mode to the TE slab mode).

B. TM-Mode Loss Mechanism

The reason for the fact that the TM mode experiences less curvature loss than does the TE mode becomes clear when a simple effective-index model is considered for the curved waveguide.

The thick solid curve in Fig. 3 shows schematically the equivalent index profile $n_{\mathrm{eq,TE}}(x)$ for the TE modes of the rib waveguide shown in Fig. 1, where the tilt of the profile represents the curvature of the rib waveguide [18]. The thin solid line indicates the effective index $n_{\mathrm{eff,TE}}$ of the fundamental TE waveguide mode. According to a Wentzel–Kramers–Brillouin analysis, the curvature loss of this mode is mainly proportional to $\exp(-I)$, where

$$I = \frac{2\pi}{\lambda} \int_{W/2}^{x_{\mathrm{c,TE}}} \sqrt{n_{\mathrm{eff,TE}}^2 - n_{\mathrm{eq,TE}}(x)^2}\, dx \qquad (1)$$

is an integral over the spatial region where the field is purely evanescent [18]. This region extends from the core-cladding boundary at $x = W/2$ to the TE caustic at $x = x_{\mathrm{c,TE}}$. Light must tunnel through this barrier (the strength of which is characterized by I) into the oscillation region beyond the caustic. The tunnel barrier has been visualized as the triangular area labeled "1" in Fig. 3; it is enclosed by the effective-index line $n_{\mathrm{eff,TE}}$ and the equivalent index profile $n_{\mathrm{eq,TE}}(x)$.

Analogously, the thick dotted curve in Fig. 3 shows the equivalent index profile $n_{\mathrm{eq,TM}}(x)$ for the TM modes, and the thin dotted line indicates the TM-mode effective index $n_{\mathrm{eff,TM}}$. Here, the curvature-loss tunnel barrier is the triangular area labeled "2," which is enclosed by the two curves between the core-cladding boundary and the TM caustic $x = x_{\mathrm{c,TM}}$. This area is larger than the corresponding TE area for the following reason. In the slab region ($|x| > W/2$), the equivalent index $n_{\mathrm{eq,TM}}(x)$ of the TM modes is lower than the equivalent index $n_{\mathrm{eq,TE}}(x)$ of the TE modes. The effective indices of the TE and TM waveguide modes, however, are much closer together—in a zero-birefringence waveguide, they would even coincide. It is then clear geometrically that the tunnel barrier is usually both deeper and longer for TM modes, resulting in lower curvature loss for the TM mode at the same bend radius.

However, the above discussion is not complete. We have to take into account the fact that the modes in a rib waveguide are not perfectly uniformly polarized but slightly hybrid. The presence of an orthogonal field component permits the coupling

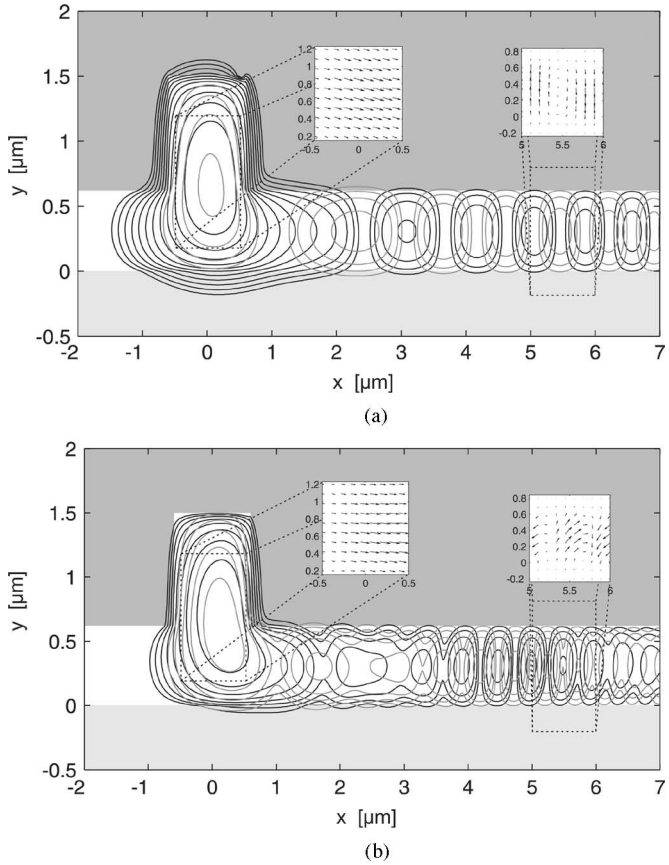

Fig. 4. Contours in steps of 2 dB of the transverse H-field magnitude of the quasi-TM mode of the waveguide marked with a cross in Fig. 2(b). The waveguide is curved to the left such that the power is radiated toward the outer, right-hand slab waveguide. *Dark* and *light* contours correspond to real and imaginary parts of the field, respectively. The insets show the real part of the transverse H-field vectors. (a) Bend radius $R = 80$ μm. (b) Bend radius $R = 30$ μm.

of the TE waveguide mode to the TM slab mode and of the TM waveguide mode to the TE slab mode. The latter case is particularly important. Analogous to the two cases in the preceding paragraphs, the loss induced by the radiation of the TM rib mode into the TE slab mode is related to the triangular area marked as "3" in Fig. 3, which is enclosed by the effective-index line $n_{\mathrm{eff,TM}}$ and the equivalent index profile $n_{\mathrm{eq,TE}}(x)$ between the core-cladding boundary and the caustic $x = x_{\mathrm{c,TETM}}$ (this area is simply the intersection of the other two areas "1" and "2"). It can be seen in Fig. 3 that this tunnel barrier is particularly small and, thus, enables an efficient radiation mechanism for the TM rib mode, even when the hybridicity of the rib mode is very small. The cross-polarization coupling from the TE waveguide mode to the TM slab mode can be neglected, because the corresponding tunnel barrier is much higher than that of the coupling to the TE slab mode.

C. Illustration of Curvature Loss Mechanisms

In this section, we illustrate the coupling of the curved TM waveguide mode to the TE slab mode. As an example, we pick

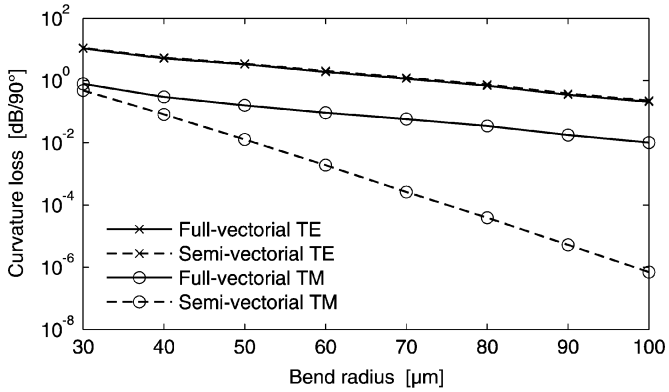

Fig. 5. Ninety-degree curvature loss versus bend radius for the waveguide marked with a cross in Fig. 2(b). While TE-mode losses are described well by a semi-vectorial model, TM-mode losses require a full-vectorial description due to cross-polarization radiation.

the waveguide marked with a cross in Fig. 2(b): $H = 1.5$ μm, $D = 0.88$ μm, $W = 1.2$ μm.

That the coupling of the TM rib mode to the TE slab mode is indeed significant is shown in Fig. 4(a), where the transverse H-field of the quasi-TM mode in the rib waveguide marked with a cross in Fig. 2(b) has been plotted for the bend radius $R = 80$ μm. The radiation of power into the slab waveguide can be clearly seen—toward the outside, the phase of the mode field increases, such that the phase fronts of the propagating wave lag behind those inside the core and power is radiated away. The insets in Fig. 4(a) show the vector character of the transverse H-field in the core region and in the outer slab. Even though the core field is predominantly parallel to the x-axis (quasi-TM mode), the slab carries away power mainly in the TE mode, which means that the main loss mechanism is coupling to the orthogonally polarized slab mode, as discussed in Section III-B.

For shorter bending radii, the tunneling barrier to the TM slab mode becomes increasingly shorter, and eventually the TM slab mode also carries a substantial part of the radiated power. Fig. 4(b) shows the mode field of the same waveguide as in Fig. 4(a) for a bending radius of $R = 30$ μm, where now the beating between the TE and TM slab modes can be clearly seen.

D. Insufficiency of Semi-Vectorial Modeling

As another illustration of the significance of TE-slab-mode radiation for TM rib modes, in Fig. 5, we have plotted the curvature losses of the TE and TM rib modes versus the bending radius, calculated with both full-vectorial and semi-vectorial formalisms. For the TE mode, the difference between full-vectorial and semi-vectorial calculations is relatively small. However, the TM rib-mode losses are significantly underestimated by the semi-vectorial calculations. The reason for this is that the semi-vectorial TM calculation cannot, by definition, take into account the coupling to the TE slab mode. Therefore, it does not allow for the main loss mechanism and simply yields too-low loss values.

Incidentally, this cross-polarization radiation is not the dominant loss mechanism in the GaAs/AlGaAs rib-waveguide structures from [19], [20], which are often used as benchmarks

for curvature-loss calculations [12]–[15]. The results for the curvature losses given in [12]–[15] are also accurately reproduced by the mode solver used for the present paper. However, there is practically no difference between the semi-vectorial and full-vectorial simulations when applied to the waveguides of [12]–[15], neither for the quasi-TE modes nor for the quasi-TM modes. In those rib waveguides, the quasi-TE rib mode radiates primarily into the TE slab mode and the quasi-TM rib mode radiates primarily into the TM slab mode, as opposed to the silicon-on-insulator structure analyzed in this paper.

IV. Conclusion

We have shown that the curvature loss of the quasi-TM mode in silicon rib waveguides can be significantly lower than that of the quasi-TE mode. An integrated photonic device making use of only the quasi-TM mode could therefore be shrunk to a much smaller footprint. We have shown that the slight hybridicity of the quasi-TM rib mode enables the coupling to the orthogonally polarized TE slab mode, which can be the main curvature-loss mechanism. The vectorial nature of this process makes full-vectorial simulation models essential for the accurate simulation and design of waveguides with low TM curvature loss.

References

[1] Y. A. Vlasov and S. J. McNab, "Losses in single-mode silicon-on-insulator strip waveguides and bends," *Opt. Express*, vol. 12, no. 8, pp. 1622–1631, Apr. 2004.

[2] W. Bogaerts, P. Dumon, P. Jaenen, J. Wouters, S. Beckx, V. Wiaux, D. V. Thourhout, D. Taillaert, B. Luyssaert, and R. Baets, "Silicon-on-insulator nanophotonics," in *Proc. SPIE Integr. Opt. Theory Appl.*, 2005, vol. 5956, pp. 181–195.

[3] T. Tsuchizawa, K. Yamada, H. Fukuda, T. Watanabe, J. Takahashi, M. Takahashi, T. Shoji, E. Tamechika, S. Itabashi, and H. Morita, "Microphotonics devices based on silicon microfabrication technology," *IEEE J. Sel. Topics Quantum Electron.*, vol. 11, no. 1, pp. 232–240, Jan./Feb. 2005.

[4] R. A. Soref, J. Schmidtchen, and K. Petermann, "Large single-mode rib waveguides in GeSi–Si and Si-on-SiO_2," *IEEE J. Quantum Electron.*, vol. 27, no. 8, pp. 1971–1974, Aug. 1991.

[5] B. Jalali, S. Yegnanarayanan, T. Yoon, T. Yoshimoto, I. Rendina, and F. Coppinger, "Advances in silicon-on-insulator optoelectronics," *IEEE J. Sel. Topics Quantum Electron.*, vol. 4, no. 6, pp. 938–947, Nov./Dec. 1998.

[6] S. P. Chan, C. E. Png, S. T. Lim, G. T. Reed, and V. M. N. Passaro, "Single-mode and polarization-independent silicon-on-insulator waveguides with small cross section," *J. Lightw. Technol.*, vol. 23, no. 6, pp. 2103–2111, Jun. 2005.

[7] M. Loncar, T. Doll, J. Vuckovic, and A. Scherer, "Design and fabrication of silicon photonic crystal optical waveguides," *J. Lightw. Technol.*, vol. 18, no. 10, pp. 1402–1411, Oct. 2000.

[8] S. J. McNab, N. Moll, and Y. A. Vlasov, "Ultra-low loss photonic integrated circuit with membrane-type photonic crystal waveguides," *Opt. Express*, vol. 11, pp. 2927–2939, 2003.

[9] W. N. Ye, D.-X. Xu, S. Janz, P. Cheben, M.-J. Picard, B. Lamontagne, and N. G. Tarr, "Birefringence control using stress engineering in silicon-on-insulator (SOI) waveguides," *J. Lightw. Technol.*, vol. 23, no. 3, pp. 1308–1318, Mar. 2005.

[10] N.-N. Feng, G.-R. Zhou, C. Xu, and W.-P. Huang, "Computation of full-vector modes for bending waveguide using cylindrical perfectly matched layers," *J. Lightw. Technol.*, vol. 20, no. 11, pp. 1976–1980, Nov. 2002.

[11] M. Krause, H. Renner, A. Harke, J. Müller, and E. Brinkmeyer, "Leakage loss in trench-bulge waveguides," *J. Lightw. Technol.*, vol. 23, no. 5, pp. 1890–1895, May 2005.

[12] T. Yamamoto and M. Koshiba, "Numerical analysis of curvature loss in optical waveguides by the finite-element method," *J. Lightw. Technol.*, vol. 11, no. 10, pp. 1579–1583, Oct. 1993.

[13] J.-S. Gu, P.-A. Besse, and H. Melchior, "Method of lines for the analysis of the propagation characteristics of curved optical rib waveguides," *IEEE J. Quantum Electron.*, vol. 27, no. 3, pp. 531–537, Mar. 1991.

[14] D. Dai and S. He, "Analysis of characteristics of bent rib waveguides," *J. Opt. Soc. Amer. A*, vol. 21, no. 1, pp. 113–121, Jan. 2004.

[15] W. Berglund and A. Gopinath, "WKB analysis of bend losses in optical waveguides," *J. Lightw. Technol.*, vol. 18, no. 8, pp. 1161–1166, Aug. 2000.

[16] F. Collino and P. Monk, "The perfectly matched layer in curvilinear coordinates," *SIAM J. Sci. Comput.*, vol. 19, no. 6, pp. 2061–2090, Nov. 1998.

[17] Y.-C. Chiang, Y.-P. Chiou, and H.-C. Chang, "Improved full-vectorial finite-difference mode solver for optical waveguides with step-index profiles," *J. Lightw. Technol.*, vol. 20, no. 8, pp. 1609–1618, Aug. 2002.

[18] C. Vassallo, *Optical Waveguide Concepts*. Amsterdam, The Netherlands: Elsevier, 1991.

[19] M. W. Austin, "GaAs/GaAlAs curved rib waveguides," *IEEE J. Quantum Electron.*, vol. QE-18, no. 4, pp. 795–800, Apr. 1982.

[20] R. J. Deri and R. J. Hawkins, "Polarization, scattering and coherent effects in semiconductor rib waveguide bends," *Opt. Lett.*, vol. 13, no. 10, pp. 922–924, Oct. 1988.

Michael Krause (S'03) received the Dipl.-Ing. degree in electrical engineering from the Technische Universität Hamburg-Harburg (TUHH), Hamburg, Germany, in 2003. He is currently working toward the Dr.-Ing. degree in the Department of Optical Communication Technology, TUHH.

His current research interests include Raman amplification and lasing in optical fibers and silicon waveguides, and waveguide theory.

Hagen Renner received the Dipl.-Ing. and Dr.-Ing. degrees from the Technical University of Dresden, Dresden, Germany, in 1985 and 1990, respectively, both in electrical engineering.

Since 1991, he has been with the Technische Universität Hamburg-Harburg, Hamburg, Germany, where he is currently a Senior Engineer in the Optical Communication Technology group. His current research interests include fiber and integrated optics, waveguide design, Bragg gratings, and Raman scattering in fibers and silicon waveguides.

Ernst Brinkmeyer received the Diploma and Doctoral degrees in physics from the University of Göttingen, Göttingen, Germany, in 1973 and 1976, respectively.

He is currently a Professor in the Electrical Engineering Department, Technische Universität Hamburg-Harburg, Hamburg, Germany, where he heads the Optical Communication Technology group. His current research interests include optical communications and optical instrumentation, in particular, Raman amplification, fiber Bragg gratings and planar UV-written structures, PMD compensation, and silicon photonics.